is possible that the negative entropy term is the result of a positive entropy contribution accompanying a dissociative process being offset by a solvation requirement for the incipient BH_3 group and free amine in the transition state.

Previous applications of the Hammett equation to reactions of quinoline derivatives have included a study of variations of reactivity, with position, of side-chain acid and ester functions.[23] Its application here must be considered with caution inasmuch as this linear free-energy relationship is designed for correlation of rates and equilibria of reactions occurring at aryl side chains. Nevertheless, a correlation of kinetic data for 3- and 4-substituted quinoline–boranes is probably not surprising if one considers the primary reaction site to be the electron pair of the B–N bond, and although quinoline–borane hydrolysis is quite sensitive to electronic inductive effects of hetero ring substituents ($\rho = 3.4$ for the acid-independent contribution), there appears to be no imposition of electronic demand that would necessitate the use of modified substituent constants beyond those σ values which are defined on the basis of benzoic acid dissociation.[18,20,24-27]

The effect of the 2-methyl group in producing an approximate 30-fold increase in k_1, relative to unsubstituted quinoline–borane, is attributed to steric enhancement of a dissociative pathway involving a change in the coordination number of nitrogen from four in the amine–borane to three in the incipient free amine. Interestingly, 2-methyl substitution also causes a greater than 2-fold *increase* in k_2, presumably reflecting the greater importance of the electronic inductive effect of the methyl group over its capacity to hinder approach of solvated proton to the coordination sphere of nitrogen. A small effect on k_1 and k_2 is also observed on introduction of methyl or methoxy in the 6-position, suggesting some transmission of electronic induction from this region of the all-carbon ring. The nearly 20-fold increase in k_1 resulting from insertion of a nitro group at this position is consistent with previous reports of the exceptional effect of the NO_2 function in reactions subject to acceleration by electron-withdrawing substituents, particularly where there is direct conjugation of the nitro group with the reaction site.[27]

It is also interesting to compare kinetic parameters of quinoline–borane and its derivatives with those of isoquinoline–borane. Relative values of k_1 and k_2 suggest, for the quinoline–boranes, a steric influence of the peri hydrogen at C-8, resulting in enhancement of the dissociative pathway and, to a lesser degree, retardation of bimolecular substitution relative to what is exhibited by the isoquinoline derivative. Such an influence is further suggested by the magnitude of the k_1 term in 8-methylquinoline–borane.

These studies provide insight regarding the effects of substituents on the stability of heteroaromatic amine–boranes in protic media. Recognition of these factors is essential to extending the potential synthetic utility of the amine–borane moiety as a convenient protecting group for tertiary nitrogens.[2]

Acknowledgment. Support of The Robert A. Welch Foundation (Grant P-162) and the TCU Research Fund is gratefully acknowledged.

Registry No. Quinoline–*N*-borane, 13240-36-3; 2-methylquinoline–*N*-borane, 92367-41-4; 3-methylquinoline–*N*-borane, 54304-40-4; 4-methylquinoline–*N*-borane, 94553-41-0; 6-methylquinoline–*N*-borane, 102941-75-3; 8-methylquinoline–*N*-borane, 54304-36-8; 3-bromoquinoline–*N*-borane, 102941-76-4; 4-chloroquinoline–*N*-borane, 102941-77-5; 6-methoxyquinoline–*N*-borane, 102941-78-6; 6-nitroquinoline–*N*-borane, 102941-79-7; isoquinoline–*N*-borane, 54304-37-9.

(23) Elderfield, R. C.; Siegel, M. *J. Am. Chem. Soc.* **1951**, *73*, 5622-5628.
(24) McGary, C. W., Jr.; Okamoto, Y.; Brown, H. C. *J. Am. Chem. Soc.* **1955**, *77*, 3037-3043.
(25) Okamoto, Y.; Brown, H. C. *J. Org. Chem.* **1957**, *22*, 485-494.
(26) Brown, H. C.; Okamoto, Y. *J. Am. Chem. Soc.* **1958**, *80*, 4979-4987.
(27) Jaffe, H. H. *Chem. Rev.* **1953**, *53*, 191-261.

Contribution from the Max-Planck-Institut für Strahlenchemie and Max-Planck-Institut für Kohlenforschung, D-4330 Mülheim a. d. Ruhr, West Germany, Institut für Theoretische Chemie, Universität Düsseldorf, D-4000 Düsseldorf, West Germany, and Faculty of Science, Rikkyo University, Nishiikebukuru 3, Toshima-ku, Tokyo 171, Japan

Vibrational Fine Structure of the Lowest Spin-Allowed Absorption Band of *trans*-$[Co(CN)_2(tn)_2]^+$ (tn = 1,3-Propanediamine). Structures of *trans*-$[Co(CN)_2(tn)_2]Cl\cdot H_2O$ and *trans*-$[Co(CN)_2(tn)_2]Cl\cdot 3H_2O$

Hans Kupka,*† Joachim Degen,‡ Akio Urushiyama,§ Klaus Angermund,∥ and Carl Krüger∥

Received December 5, 1985

The results of X-ray structure analyses of *trans*-$[Co(CN)_2(tn)_2]Cl\cdot H_2O$ and *trans*-$[Co(CN)_2(tn)_2]Cl\cdot 3H_2O$ are presented. In these crystal lattice systems the cationic complex exists in two forms. In the trihydrate crystal both six-membered metal chelate rings of the complex ion *trans*-$[Co(CN)_2(tn)_2]^+$ assume the chair form, while in the monohydrate crystal one is present in the chair and the other one in the skew-boat form. This change in geometry of the complex ion is made manifest by high-resolution, polarized absorption spectroscopy. This shows that the spectrum of the monohydrate yields much less information in the region of the lowest spin-allowed transition $^1A(C_1)[^1A_{2g}(D_{4h})] \leftarrow {}^1A$ than does the spectrum of the $^1B_g(C_{2h})[^1A_{2g}(D_{4h})] \leftarrow {}^1A_g$ transition in the trihydrate crystal. Analysis of the vibronic structure in these spectral regions, supported by the results of a normal-coordinate analysis, shows that the complex ion undergoes a distortion in its electronic excited state ^1B_g (trihydrate) and ^1A (monohydrate). This results in a flattening of the chelate rings in the equatorial direction, as well as a contraction along the vertical axis containing the cyanide ligands. This flattening produces an expansion of ~0.06 Å in the Co–N bond lengths. Support for the experimentally determined excited-state distortion is provided by MO calculations of the forces exerted in the excited state of *trans*-$[Co(CN)_2(tn)_2]^+$.

I. Introduction

In previous studies,[1,2] we had estimated the distortion of *trans*-$[Co(CN)_2(NH_3)_4]^+$ and *trans*-$[Co(CN)_2(en)_2]^+$ in their ligand field excited states $^1A_{2g}(D_{4h})$ and $^1B_g(C_{2h})[^1A_{2g}(D_{4h})]$, respectively. This was done through analysis of the vibrational fine structure and the intensity distribution of the single-crystal absorption bands combined with a normal-coordinate analysis of the distorting (accepting) modes of the chromophores. It was found that the *trans*-$[Co(CN)_2(en)_2]^+$ complex undergoes dis-

† Max-Planck-Institut für Strahlenchemie.
‡ Universität Düsseldorf.
§ Rikkyo University.
∥ Max-Planck-Institut für Kohlenforschung.

(1) Urushiyama, A.; Kupka, H.; Degen J.; Schmidtke, H.-H. *Chem. Phys.* **1982**, *67*, 65.
(2) Hakamata, K.; Urushiyama, A.; Degen, J.; Kupka, H.; Schmidtke, H.-H. *Inorg. Chem.* **1983**, *22*, 3519 and references cited therein.

0020-1669/86/1325-3294$01.50/0

tortion only in the totally symmetric δ (en cycle) mode, which is made up primarily of Co–N and N–C stretching vibrations with some N–Co–N deformations. This produces a change in the geometry of the complex in its excited state ^1B_g relative to the ^1A_g ground state, resulting in a motion outward of the ethylenediamine ligands along the $y + z$ molecular axes. At the same time, the change in the Co–N bond length was $\Delta r = 0.06$ Å. Other distorting modes (among the nine totally symmetric modes) involving comparable amounts of Co–N stretching as well as mode mixing could not be detected with certainty.

In the present study, these investigations are extended to molecular crystals of dicyano complexes consisting of six-membered chelate rings, *trans*-$[Co(CN)_2(tn)_2]^+$ (tn = 1,3-propanediamine). The complex exists in the crystalline form in two modifications, in which the rings are forced to adopt different puckered equilibrium conformations. This will be described in section III, where the geometrical structures of *trans*-$[Co(CN)_2(tn)_2]^+$ in *trans*-$[Co(CN)_2(tn)_2]Cl\cdot H_2O$ and *trans*-$[Co(CN)_2(tn)_2]Cl\cdot 3H_2O$ are discussed. After we describe briefly the details of the experimental procedure in section II, the electronic spectra and their description are presented in section IV. Next, the vibrational (infrared and Raman) spectra are recorded for the purpose of calculating force constants and to assign the fundamental frequencies of the *trans*-$[Co(CN)_2(tn)_2]^+$ ion. In section V, MO calculations of the distorting forces are carried out and finally, by combining results of these calculations with the analysis of the intensity distribution in the electronic spectra, the excited-state geometries of *trans*-$[Co(CN)_2(tn)_2]^+$ in both crystal systems are estimated.

II. Experimental Section

The compound *trans*-$[Co(CN)_2(tn)_2]Cl\cdot H_2O$ was prepared by using the method described by Kawaguchi et al.[3] The crystals were grown by slow evaporation of an aqueous solution at 23 °C. Anal. Calcd. for $[Co(CN)_2(tn)_2]Cl\cdot H_2O$: C, 30.73; H, 7.09; N, 26.88. Found: C, 30.52; H, 7.29; N, 25.85. The crystal obtained at 5 °C from the aqueous solution of the monohydrate saturated at 30 °C was the chloride trihydrate *trans*-$[Co(CN)_2(tn)_2]Cl\cdot 3H_2O$, as confirmed by X-ray analysis (see Section III). The trihydrate crystals grew in rhombic plates under these conditions of crystallization. N and O deuterations of the trihydrate crystal were accomplished by twice recrystallization from D_2O. Upon complete deuteration of the four amino groups of the *trans*-$[Co(CN)_2(tn)_2]^+$ complex the infrared and Raman spectra change and differ in some regions from those of the undeuterated ones (Table III). The trihydrated crystal is extremely sensitive in air at ordinary temperature and releases crystal water to give a brownish yellow residue without transparency. Below 8 °C the crystals are stable and can be retained indefinitely under these conditions.

The methods and apparatus used for measurements of the single-crystal polarized absorption spectra in a temperature range from 300 to 4.2 K were for the most part similar to those used previously.[2] The spectral range extended from 17 500 to 28 500 cm^{-1}. Furthermore, for low-temperature investigation a new apparatus was constructed from an ordinary liquid-helium metal Dewar and a 0.5-m Jasco CT-50 monochromator equipped with a HPN C 767 photocounting system. The monochromatic light was introduced from the top into the Dewar through a flexible light guide (Mitsubishi Lumica). In the Dewar a specially designed sample holder was immersed in liquid He. The single-crystal sample covered a small hole (ϕ = 1 mm) in an aluminum plate that was placed just below the exit of the light guide. The transmitted light was guided to the photon counter. A small cut piece of film polarizer was successfully used even at 4.2 K.

Infrared, absorption spectra of the solids were recored on Perkin-Elmer 325, JASCO A 220, and JASCO IR-F infrared spectrometers as Nujol

(3) Kawaguchi, H.; Kawaguchi, S. *Bull. Chem. Soc. Jpn.* **1973**, *46*, 3453.
(4) In addition to several locally written programs, the following programs were used: TRACER by Lawton and Jacobson for cell reduction; DATAP by Coppens, Leiserowitz, and Rabinovich for data reduction; DIFABS by Walker and Stuart for empirical absorption correction; Sheldrick's SHELX-76/84 for Fourier calculations and initial least-squares refinement; GFMLS, an extensively modified version of ORFLSD, by Hirshfeld, Coppens, Leiserowitz, and Rabinovich for subsequent full-matrix least-squares refinement; Davis' DAESD for bond distance and angle calculations; Roberts and Sheldrick's XANADU for best plane and torsion angle calculations; Johnson's ORTEP for the molecular drawings. *International Tables for X-ray Crystallography*; Kynoch: Birmingham, England, 1974; Vol. IV.

Table I. Data for X-ray Diffraction of *trans*-$[Co(CN)_2(1,3\text{-}tn)_2]Cl\cdot H_2O$

(A) Crystal Data	
formula: $C_8H_{22}OClCoN_6$	a = 18.737 (1) Å
cryst syst: orthorhombic	b = 12.161 (1) Å
M_r: 312.7	c = 11.660 (2) Å
space group: *Pbca* (No. 61)	$\alpha = \beta = \gamma = 90°$
cryst size: 0.25 × 0.54 × 0.40 mm	Z = 8
d_c = 1.56 g cm^{-3}	V = 2656.9 Å^3

(B) Data Measurement
diffraction: Nonius CAD4
radiation: Mo Kα (λ = 0.71069 Å)
monochromator: graphite
scan mode: Ω–2θ
no. of refl measd: 5443 ($\pm h, +k, +l$)
abs cor: μ(Mo Kα) = 14.87 cm^{-1}; empirical cor applied
R_{av}: 0.01
no. of independent refl: 2991
no. of obsd refl: 2389 ($I \geq 2.0\sigma(I)$)
no. of params: 242
R = 0.023
R_w = 0.031
error of fit: 1.72
final av shift/error: 0.44
final diff Fourier: 0.27 e Å^{-3}

Table II. Selected Bond Distances (Å) and Angles (deg)[4]

Distances			
Co–N1	1.990 (2)	N3–C4	1.490 (2)
Co–N2	1.997 (1)	N4–C6	1.484 (2)
Co–N3	1.980 (1)	N5–C7	1.148 (2)
Co–N4	1.982 (1)	N6–C8	1.157 (2)
Co–C7	1.927 (2)	C1–C2	1.505 (3)
Co–C8	1.930 (2)	C2–C3	1.523 (3)
N1–C1	1.488 (3)	C4–C5	1.514 (3)
N2–C3	1.483 (3)	C5–C6	1.522 (3)

Angles			
N1–Co–N2	89.9 (1)	C7–Co–C8	178.6 (1)
N1–Co–N3	175.4 (1)	Co–N1–C1	115.0 (1)
N1–Co–N4	91.1 (1)	Co–N2–C3	117.8 (1)
N1–Co–C7	85.7 (1)	Co–N3–C4	118.4 (1)
N1–Co–C8	93.1 (1)	Co–N4–C6	119.8 (1)
N2–Co–N3	90.1 (1)	N1–C1–C2	112.5 (2)
N2–Co–N4	175.8 (1)	C1–C2–C3	115.5 (2)
N2–Co–C7	91.6 (1)	N2–C3–C2	113.3 (2)
N2–Co–C8	87.6 (1)	N3–C4–C5	112.9 (1)
N3–Co–N4	89.3 (1)	C4–C5–C6	114.3 (2)
N3–Co–C7	89.7 (1)	N4–C6–C5	111.6 (1)
N3–Co–C8	91.5 (1)	Co–C7–N5	176.8 (1)
N4–Co–C7	92.5 (1)	Co–C8–N6	179.4 (1)
N4–Co–C8	88.3 (1)		

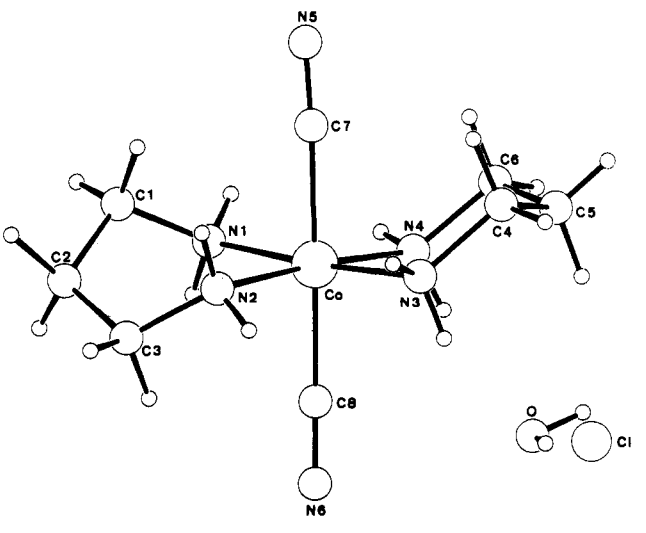

Figure 1. Molecular structure of *trans*-$[Co(CN)_2(tn)_2]Cl\cdot H_2O$.

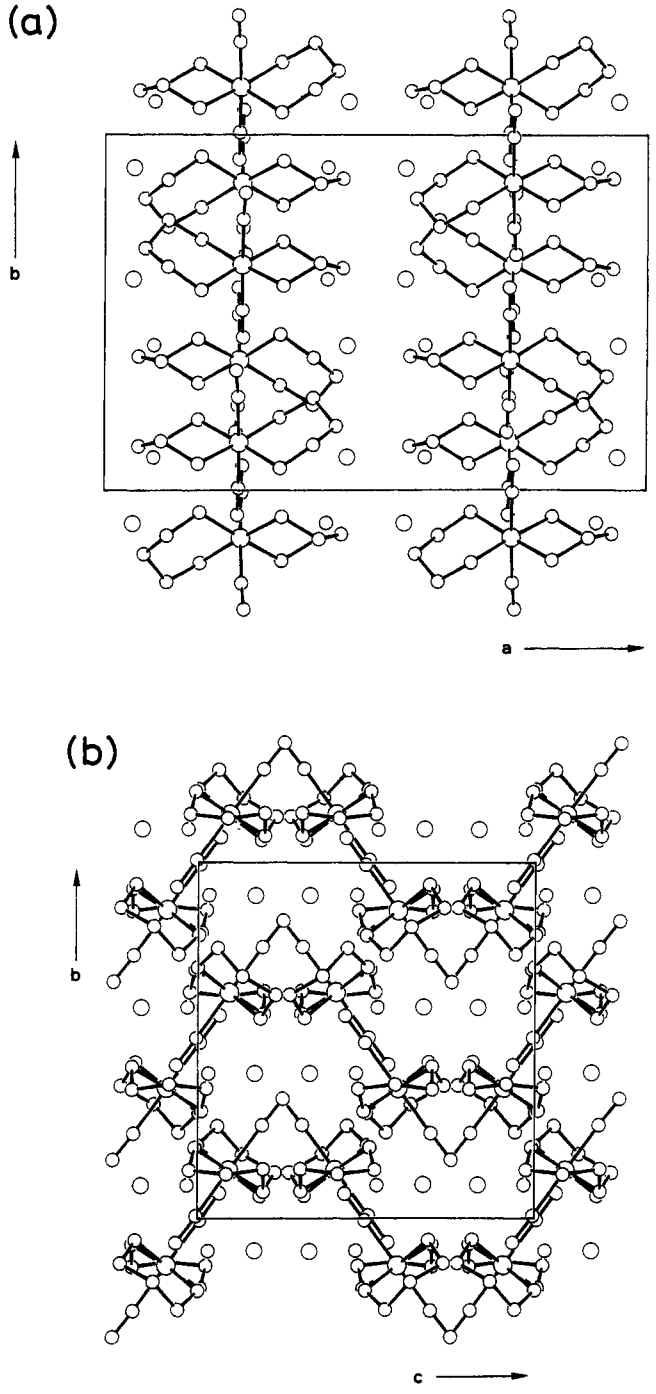

Figure 2. Crystal packing of *trans*-$[Co(CN)_2(tn)_2]Cl{\cdot}H_2O$: (a) projection on plane *ab* (view down the *c* axis). (b) projection on plane *bc* (view down the *a* axis).

mulls. The Raman spectra were studied with a Narumi 1200 ZA spectrometer and He–Ne (6.328 nm) excitation was used, with the unstable trihydrates cooled to liquid-nitrogen temperature during excitation. The incident exciting beam was angled 45° to the crystal face and polarized, such that the electric vector was parallel to the longer diagonal of the rhombic crystal face. The scattered intensity was taken at 90° to that of the incident radiation. The measurement on the monohydrate was done by employing the ordinary powder technique at room temperature.

III. Description of the Structure

The structure of *trans*-$[Co(CN)_2(tn)_2]Cl{\cdot}H_2O$ has been determined by X-ray diffraction. Experimental data are summarized in Table I. Table II contains selected bond distances and angles.

The cationic complex (Figure 1) forms a distorted octahedron (C_1 symmetry), in which the cyano groups occupy the axial positions. The equatorially coordinated diamine ligands form

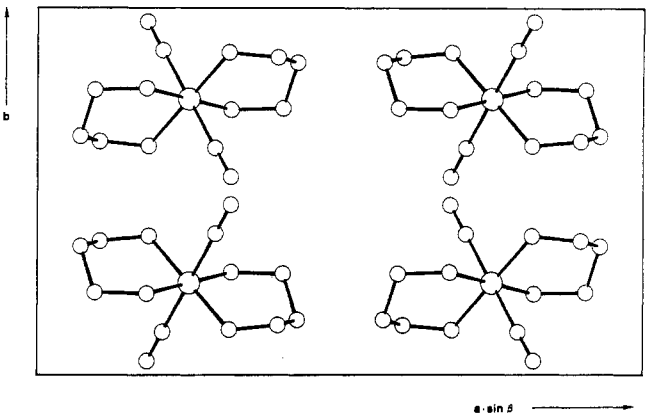

Figure 3. Crystal packing of *trans*-$[Co(CN)_2(tn)_2]Cl{\cdot}3H_2O$: view down the *c* axis.

six-membered metallacycles, one of which assumes a chair conformation (ligand containing N3 and N4), while the other adopts a twist or skew-boat conformation (ligand containing N1 and N2). Bond distances and angles correspond to those found in various similar compounds.

Figure 2 shows two projections of the contents of the unit cell. In the crystal the molecules are stacked collinearly to the crystallographic *b* axis (Figure 2a), while the NC–Co–CN axis (or strictly the straight line connecting the N5 and N6 atoms) occurs in two different orientations with respect to the unit cell (see Figure 2b). In the first case the axis is inclined to the (*a*,*b*), (*a*,*c*), and (*b*,*c*) planes at angles of 36.7, 53.3, and 0.7°, respectively, while in the second orientation the angles amount to 143.3, 126.7, and 179.3°.

A crystal structure analysis of a related compound containing 3 mol of H_2O was hampered by disorder of Cl anions and water molecules. Therefore, only some information about the cationic complex and its packing in the crystal is presented. In Figure 3 the slightly distorted octahedrons (C_{2h} symmetry) are depicted with the CN groups in axial and the two chelating ligands in equatorial positions. Both rings adopt a chair conformation; the NC–Co–CN axis again occurs in two different orientations with respect to the unit cell.

IV. Electronic Spectroscopy

A. Absorption Spectra. The polarized absorption spectra of *trans*-$[Co(CN)_2(tn)_2]Cl{\cdot}3H_2O$ and *trans*-$[Co(CN)_2(tn)_2]Cl{\cdot}H_2O$ at 4.2 K are shown in Figures 4 and 5, respectively. The spectra were measured with an incident exiting beam at right angle to the crystal faces, which were predominantly developed from the aqueous solution. In the case of the monohydrate, the c spectrum was recorded with incident light polarized parallel to the crystallographic *c* axis, and the b spectrum as measured with light for which the electric vector was parallel to the *b* axis of the crystal. As the crystallographic axes of *trans*-$[Co(CN)_2(tn)_2]Cl{\cdot}3H_2O$ at this stage were not identified by X-ray diffraction, the polarizations of the incident radiation were aligned at extinction directions that are parallel to the diagonals of the rhombic crystal face (see Experimental Section).

In analogy with the previously reported work on *trans*-$[Co(CN)_2(NH_3)_4]^+$[1] and *trans*-$[Co(CN)_2(en)_2]^+$,[2] the smoothed absorption band with a maximum at 24 200 cm^{-1} of the monohydrate (Figure 5) corresponds to the transitions ^1A, $^1A(C_1)[^1E_g(D_{4h})] \leftarrow {}^1A(C_1)[^1A_{1g}(D_{4h})]$. Each of these two neighboring electronic levels gives rise to vibronic bands, which overlap and cannot be separated. The band with the vibronic structure in the low-energy region, 18 500–22 500 cm^{-1}, is assigned to the $^1A(C_1)[^1A_{2g}(D_{4h})]$ ligand field states. The corresponding transitions in the trihydrate crystal (Figure 4) are ^1B_g, $^1A_g(C_{2h}) \leftarrow {}^1A_g(C_{2h})$ and $^1B_g(C_{2h}) \leftarrow {}^1A_g(C_{2h})$, respectively.

In the spectra of *trans*-$[Co(CN)_2(tn)_2]Cl{\cdot}3H_2O$ (Figure 4) the predominant peaks appear at 18 506, 18 706, 18 906, 19 106, 19 318, 19 523, 19 730, ... cm^{-1}, the intervals between them being 200, 200, 200, 212, 215, 207, ... cm^{-1}. Furthermore, it is noticeable

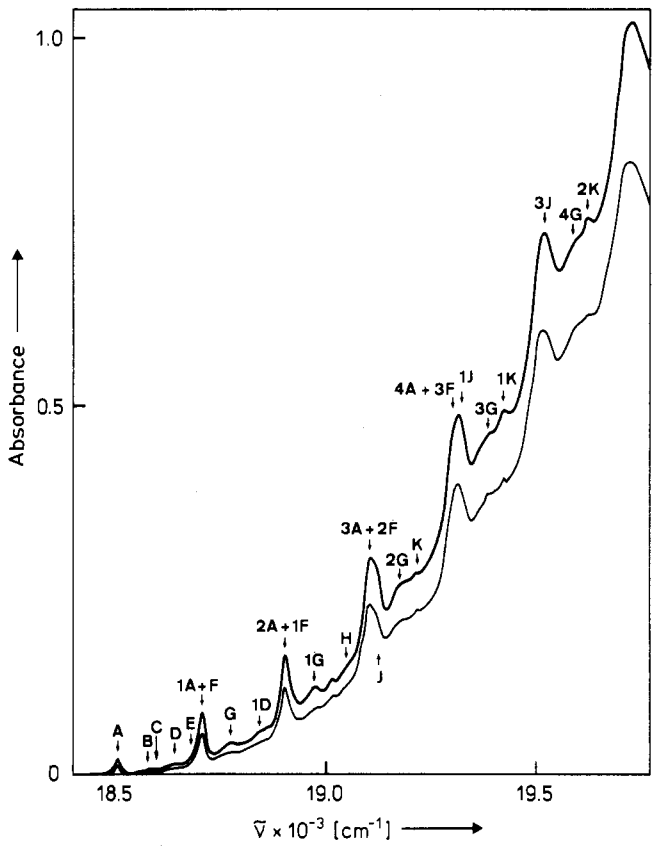

Figure 4. Low-energy region of the $^1B_g \leftarrow {}^1A_g$ polarized absorption band of *trans*-$[Co(CN)_2(tn)_2]Cl \cdot 3H_2O$ at 4.2 K, at extinction directions in the rhombic crystal face parallel to the longer diagonal (heavy line) and to the shorter diagonal (thin line); see text (crystal thickness 0.60 mm).

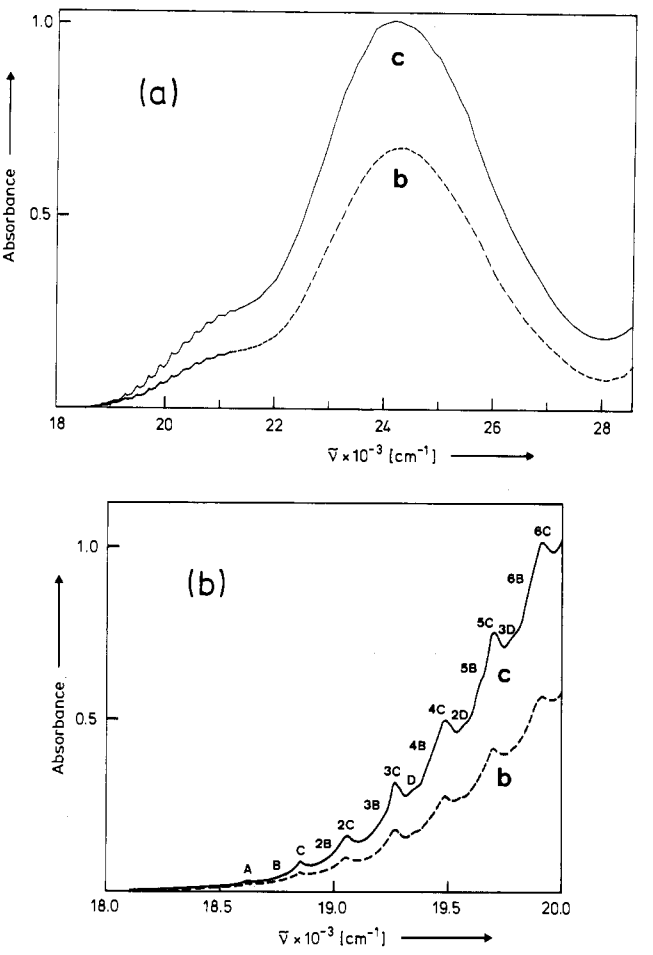

Figure 5. (a) Overall absorption spectrum of the transitions ^1A, $^1A[^1E_g(D_{4h})] \leftarrow {}^1A[^1A_{1g}(D_{4h})]$ in *trans*-$[Co(CN)_2(tn)_2]Cl \cdot H_2O$ at 4.2 K measured by incident radiation polarized parallel to the *b* and *c* crystallographic axes (crystal thickness 0.054 mm). (b) Low-energy region of the $^1A \leftarrow {}^1A$ absorption band showing the first members of the 215-cm^{-1} progressional mode. Clearly visible are also the three vibronic origins B, C, and D (crystal thickness 0.39 mm).

that the components higher than 19 106 cm^{-1} have strikingly wider half-widths compared to those at 18 506, 18 706, and 18 906 cm^{-1}. The component at 19 106 cm^{-1} has a shoulder on the higher frequency side. This component gains gradually in relative intensity in the higher frequency region to yield resolvable peaks. No other vibronic component has been detected below 18 500 cm^{-1} at 4.2 K. The deuterated compound, *trans*-$[Co(CN)_2(d_4\text{-N-tn})_2]Cl \cdot 3D_2O$, showed a pattern of the spectra similar to those of the H compound, but with a reduced interval in the progression of 195 cm^{-1}.

On the basis of these characteristics observations the vibrational fine structure can be interpreted as follows: Component A is of pure electronic origin while the components B, C, ..., and K are vibronic origins of the transition. The energy intervals between A and each vibronic origin range from 0 to 620 cm^{-1}, so that these vibronic components (except for the K component) can be attributed to lattice modes and to skeletal deformational modes of the complex. Detailed assignments are not possible because many odd parity modes involved in the vibronic mechanism of this transition can appear in this region. However, the component K can reasonably well be correlated to the ring deformational mode (C–C stretch), which is found by calculation to have a vibrational energy of 722 cm^{-1} in the electronic ground state. The components nA, nB, ..., nK, nX = $\nu_X' + n\nu_\delta$ (X = A, ..., K), are members in the progression in the ν_δ' total symmetric mode (of the electronic excited state) built on the origin components. The results of the intensity distribution analysis strongly suggest a hidden component F around 18 700 cm^{-1} overlapping with the first member 1A (A + 205) of the progression.

The vibrational fine structure of the band of *trans*-$[Co(CN)_2(tn)_2]Cl \cdot H_2O$ has a somewhat diffuse character (Figure 5b) and does not allow clear resolution of the vibronic lines. This is caused by vibrational congestion primarily due to the low (C_1) site symmetry of the complex in the monohydrate lattice. In such a symmetry all "internal vibrations" become potentially active in inducing electric dipole intensity, occurring with one vibrational quantum in the transition (see below). Lattice vibrations (phonons) occur only in combination with local modes. Nevertheless, a progression is clearly visible with a spacing of 215 cm^{-1} built on several components labeled by A, B, C, and D in Figure 5b. No other vibronic component could be seen below 18 500 cm^{-1}. The energy spacing between A and C amounts to 225 cm^{-1}, which does not coincide with the progressional interval of 215 cm^{-1}. The first member in the progression nD appears at 19 350 cm^{-1}; no other progressional components at lower energy than 19 135 cm^{-1} were detected even on repeated scans. From these observations, the major spectral features can be summarized as follows: component A is assigned to the pure electronic origin, and the accompanying components B, C, and D are assigned to the vibronic origins. The energy spacings between A and B and between A and C were estimated to be 150 and 230 cm^{-1}, respectively, so that these vibrations could be assigned to the skeletal deformations. A detailed assignment, however, is not possible. The lines nB and nC are members in the progression involving the 215-cm^{-1} mode (of the electronic excited state). The energy spacing between A and C is 730 cm^{-1}; this can be related to the ring deformational mode or to the (ground state) NH_2 rocking frequency of about 800 cm^{-1}.

According to these assignments, all the absorption bands corresponding to the transitions $^1A \leftarrow {}^1A(C_1)$ and $^1B_g \leftarrow {}^1A_g(C_{2h})$ can be analyzed in terms of a line shape function, as has been described previously[2,5]

$$W(\omega) = \sum_{m_\mu} f(\omega - \sum_{\mu=1}^{k} m_\mu \nu_\mu) I_k \left({}^{m_1, m_2, \ldots, m_k}_{0, 0, \ldots, 0} \left| \left\{ \Delta^{j_1, j_2, \ldots, j_q}_{i_1, i_2, \ldots, i_p} \right\} \{\beta_\mu, \beta_{\mu\eta}\} \right. \right) \quad (1)$$

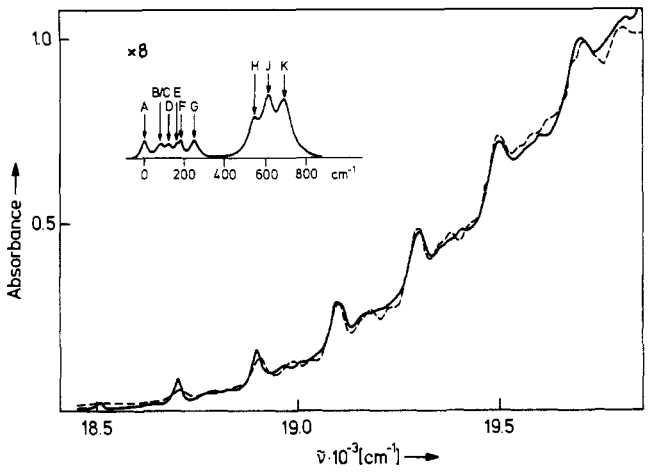

Figure 6. Calculated fit to experimental $^1B_g \leftarrow {}^1A_g$ absorption spectrum of *trans*-$[Co(CN)_2(tn)_2]Cl{\cdot}3H_2O$ (heavy solid line of Figure 4). The insert is the sideband function $f(\omega)$.

where $f(\omega)$ is a sideband function describing the predicted vibronic structure (A, B, C, ..., and H lines) in the region around the pure electronic origin and m_μ and ν_μ' are the excited-state vibrational quantum numbers and the vibrational frequencies of the progressional modes. The prime on ν_μ stand for excited state. As the measurement was done at low temperature, the ground-state vibrational quantum number $n_1 = n_2 ... = n_k = 0$. The weighting factor I_k in the sum (eq 1) is an intramolecular distribution,[5] which incorporates, through the spectroscopic constants, the distortion of the electronic excited state relative to that of the ground state. Several factors have been considered here: first, the dimensionless normal mode displacements $\Delta^{\mu}_{1,2,...k}$ along the distorting modes Q_μ; second, their frequency (force constant) changes $\beta_\mu = \nu_\mu'/\nu_\mu$; third, mode mixing. The latter effect gives rise to a whole set of additional geometrical displacement parameters $\{\Delta^{j_1 j_2 ... j_q}_{i_1,i_2,...i_p}\}$ ($p < q$, $1 < q \leq k$) that are generated by the normal-coordinate rotation and to crossed frequency factors $\beta_{\mu\eta} = \nu_\mu'/\nu_\eta$.[5] The index k in I_k denotes the number of accepting (distorting) modes involved in the transition. Generally, it is reasonable to assume that k is larger than unity because, as will be shown latter, there are several local modes, which may be displaced and mixed due to coordinate rotation. However, as can be seen in Figure 6, by using a function $f(\omega)$ (the insert in the figure) representing the vibronic structure in the electronic origin region of the $^1B_g \leftarrow {}^1A_g$ transition in *trans*-$[Co(CN)_2(tn)_2]Cl{\cdot}3H_2O$, the 205-$cm^{-1}$ accepting mode (ν_δ') alone is sufficient to account for the whole $^1B_g \leftarrow {}^1A_g$ absorption band shape. This means that in our particular case the structure arising from the accepting mode ν_δ' can be analyzed in terms of a one-dimensional distribution, $I_1(m,o;\Delta_1^\delta,\beta_\delta)$. The latter depends parametrically on Δ_1^δ and β_δ, where $\Delta_1^\delta = (M_\delta\omega_\delta/\hbar)^{1/2}\Delta Q_\delta$, with ΔQ_δ being the excited-state distortion along the progressional mode Q_δ and β_δ its frequency change. The function $f(\omega)$, where ω is a variable frequency, coincides with the experimentally obtained lines A, B, ..., K in the absorption spectrum (Figure 4). A close fit to the experimental absorption band shape, for which the peak heights of these lines as well as the vibrational frequency ν_δ' and the spectroscopic parameters Δ_1^δ and β_δ have been varied, is given by $\Delta_1^\delta = 3.2$, $\nu_\delta' = 205$ cm^{-1}, and $\beta_\delta = 0.87$. From the estimated excited-state vibrational frequency ν_δ' and the measured ground-state vibrational frequency $\nu_\delta = 235$ cm^{-1}, the quotient $\beta_\delta = \nu_\delta'/\nu_\delta$ yields 0.87, which is consistent with the value obtained above.

Cross quadratic effects or mode mixing, which in general are characterized by a great deal of structure (in which it is then very difficult to distinguish between various distorting modes), have not been detected. This was simulated by means of eq 1 by using the three lowest frequency Raman-active modes of Table III (k = 3), which were considered as displaced and rotated in the ^1B_g state relative to the ^1A_g state. On the basis of this fact, we suggest that our observation on the absorption is confirmed by assuming a single-mode progression. This assumption is confirmed by the study of the vibrational spectra of the complex ion and by MO calculation of the excited-state distortion (see following section).

Table III. Observed Infrared (IR) and Raman (R) Frequencies in cm^{-1} of *trans*-$[Co(CN)_2(tn)_2]^+$, Confined Mainly to the $Co(tn)_2$ Skeleton

trihydrate cryst		monohydrate cryst
H compd	D compd	H compd
235 R (δ(tn cycle))	217 R	241 R
245 IR	230 IR	265 R
260 IR	250 IR	274 IR
292 R	271 R	290 IR
300 IR	297 IR	
352 R	330 R	315 IR
354 IR	338 IR	348 IR
376 IR	356 IR	361 IR/R
388 R	386 R	386 IR, 383 R
397 R		412 IR
	414 R	
439 IR	425 IR	420 IR/R
450 R	433 R	458 IR
460 IR		435 IR, 437 R
471 R	447 R	467 IR, 468 R
517 R	481 R	504 IR
525 IR	510 IR	520 IR, 524 R
550 IR		556 IR

It is further seen from Figures 4 and 5 that the excited-state vibronic structure is practically independent of the polarization of the incident radiation. This result is contrary to what has often been supposed from polarized spectra of crystals. The reason for this behavior lies in the nature of the electronic transitions, which in the case of the considered crystal systems is induced via a vibronic coupling mechanism (mainly associated with the skeleton deformation of the complex *trans*-$[Co(CN)_2(tn)_2]^+$). On the assumption that this mechanism gives rise to the vibronic origins B, C, ..., H off A (associated with the pure electronic origin), the electric dipole moment induced in the system by the radiation field is given by[6]

$$M_\rho = \sum_\eta \langle \Gamma_e|P_\rho V_\eta|\Gamma_g\rangle\langle \chi_0|Q_\eta|\chi_1\rangle \qquad (2)$$

where the wave functions for the excited (e) and ground (g) electronic states have been written $|\Gamma_s\chi_n\rangle$, s = e, g. Here χ_n is the harmonic oscillator wave function with all the individual oscillators in their zeroth occupational state except for the vibrationally active modes, which are in the occupational state n (here, either 1 or 0). P_ρ is the electric dipole operator measured relative to the molecular axes, V_η is the derivative of the dynamical ligand potential evaluated at the ground-state equilibrium configuration, and Q_η are normal coordinates of molecular vibrations that are active in inducing electric dipole intensity. For the sake of simplicity we have assumed closure over high-lying intermediate singlet states that are admixed to the states $|\Gamma_e\rangle$ and $|\Gamma_g\rangle$ via vibrational modes Q_η. The matrix element $\langle \Gamma_e|P_\rho V_\eta|\Gamma_g\rangle$ in eq 2 will only be nonzero if the symmetry of $P_\rho V_\eta$ is contained in the product $\Gamma_e \times \Gamma_g$. This restricts the allowed molecular modes Q_η, which give rise to a dipole field at the Co^{3+} ion of a given polarization ρ. Thus, on the assumption that the molecule has a sufficiently high symmetry and a fixed orientation in the crystallographic cell, the vibronic structure in the electronic origin region of the $\Gamma_e \leftarrow \Gamma_g$ electronic transition can most conveniently be deduced by using group-theoretical methods. In application to *trans*-$[Co(CN)_2(tn)_2]+$ in the monohydrate crystal, the molecule has a low C_1 site symmetry and therefore almost all vibrational modes are active in inducing electric dipole fields of arbitrary polarizations ρ. Furthermore, the molecules occur in the unit cell in two different orientations (i = 1, 2). Hence, when the electric

(5) (a) Kupka, H.; Polansky, O. E. *J. Chem. Phys.* **1984**, *80*, 3153. (b) Kupka, H.; Olbrich, G. *J. Chem. Phys.* **1984**, *80*, 3163; **1985**, *82*, 3975.

(6) Manson, N. B. *J. Phys. C* **1978**, *11*, 2219.

Table IV. Potential Energy Distributions for the Q_δ(tn cycle) Normal Mode[a] of *trans*-$[Co(CN)_2(tn)_2]Cl\cdot 3H_2O$

coordinate	(L^{-1})	PED/%
R_{CoN}	0.62	21
R_{NC}	0.33	5
R_{CC}	0.11	
R_{CoC}	−0.04	
$R_{C\equiv N}$	−0.02	
δ(N3CoN4)(inner chelate)[b]	−0.05	10
δ(N1CoN4)(outer chelate)	0.15	10
δ(C7CoN4)	−0.22	5
δ(C7CoN1)	0.35	5
δ(CoN3C4)	0.36	22
δ(NCC)	0.13	1
δ(CCC)	0.16	1
δ(CoC7N5)	0.32	

[a] The ν_δ vibration is observed at 235 cm^{-1}. The calculated value is 242 cm^{-1}. [b] The same numbering of the atoms as in Figure 7 is used.

dipole operator P_ρ is transformed to crystal fixed axes $P_i = P_\rho C_i$, where C_i are the corresponding direction-cosine matrices, and when the two transitions are added (which is equivalent to the summation of two spectra), eq 2 indicates immediately that the vibronic structure in the electronic origin region of the $^1A \leftarrow {}^1A$ transition will be practically unchanged by the polarization ρ of the incident radiation. In support of this we note that the dichroic ratio (see Figure 5) is only slightly larger than 1. A similar situation is valid for the trihydrate crystal with the distinction that now the Co^{3+} ion lies on a C_i site (retaining inversion). Hence, under the site group selection rule, only odd-parity fundamentals become active in inducing a dipole field at the d^n ion. Evidently, this limitation imposed on the molecular modes gives a higher structured profile of the $^1B_g \leftarrow {}^1A_g$ absorption band shape.

B. Vibrational Spectra and Normal-Coordinate Analysis. In analyzing the distortion in the lowest lying excited singlet states ^1B_g (trihydrate) and ^1A (monohydrate) along the progressional mode, we need a relationship between the normal coordinates and the internal coordinates of the nuclei in both the electronic excited and ground states. This makes it necessary to perform a calculation of the normal-coordinate analysis. Unfortunately, we have no information on the values of the excited-state vibrational frequencies (with the exception of the few frequencies detected from the absorption spectra), and we therefore restrict ourselves to the study of the ground-state vibrational (infrared and Raman) spectra of the complex ion. Table III lists the observed vibrational frequencies of the *trans*-$[Co(CN)_2(tn)_2]^+$ framework in both crystal hosts. The infrared and Raman spectra of the trihydrate crystal are different from those of the monohydrate crystal.[7] They are much simpler because a mutual exclusion between IR and Raman frequencies occurs. In the spectra of the monohydrate crystal many modes of the complex ion are simultaneously infrared- and Raman-active (due to its C_1 site symmetry). This confirms the conclusion already made above that broadening of the electronic absorption spectra (Figure 5) is caused because of vibrational congestion. Furthermore, the IR spectrum of *trans*-$[Co(CN)_2(tn)_2]Cl\cdot 3H_2O$ appears to resemble that of *trans*-$[CoCl_2(tn)_2]Cl\cdot HCl\cdot 2H_2O$[8] more than that of *trans*-$[Co(CN)_2(tn)_2]Cl\cdot H_2O$. For example, both the former contain two distinct peaks in the CH_2 rocking region (890–970 cm^{-1}), whereas the spectrum of *trans*-$[Co(CN)_2(tn)_2]Cl\cdot H_2O$ has three peaks at 890, 926, and 961 cm^{-1}. Further investigations of this subject will be presented in a forthcoming publication.

The normal-coordinate analysis has been carried out for the C_{2h} symmetrical complex by using the recently described method.[2]

Table V. Calculated Totally Symmetric Forces $F_A = F_A{}^{^1B_g} - F_A{}^{^1A_g}$ Acting Directly on Atoms A in the Lowest Excited Ligand Field State ^1B_g Relative to the Ground State ^1A_g and the Corresponding Excited-State Distortion

atom A	components of F_A along octahedral axes, au			distortion, Å		
	x_A	y_A	z_A	Δx_A	Δy_A	Δa_A
Co	0.0	0.0	0.0	0.0	0.0	0.0
N3	−0.011	0.0	0.011	0.071	0.0	−0.071
N4	0.0	−0.011	0.011	0.0	0.071	−0.071
C4	−0.018	0.019	−0.017	0.116	−0.123	0.110
C5	−0.004	−0.004	−0.003	0.025	0.025	0.019
C6	0.019	−0.018	−0.017	−0.123	0.116	0.110
C7	0.0	0.0	0.016	0.0	0.0	−0.100
N5	0.0	0.0	0.005	0.0	0.0	−0.032

As a result, the internal coordinates involved in each normal mode of vibration were calculated. The force constants were also obtained. From the point of view of the vibronic structure of the absorption spectra, the most interesting normal mode of *trans*-$[Co(CN)_2(tn)_2]^+$ is the ν_δ (tn cycle) mode. The normal-mode eigenvector for this particular mode is therefore described in some detail. Table IV lists the important internal coordinates involved in ν_δ, the distribution of the potential energy (PED) between these coordinates and the corresponding elements of the $\mathbf{L}^{-1}$ matrix. Table IV shows us that this mode (along which the excited-state geometry is shifted relative to that of the ground state) is a complex mixture primarily of CoN stretching, NC stretching, NCoN bending, and CoNC bending. Co—C≡N stretching, CCoN bending, NCC bending, and CCC bending make smaller contributions. Inspections of the signs of these coordinates in the eigenvector indicate that the NCoN inner chelate bond angles decrease and the remaining chelate bond angles increase. This suggests that the chelate ring chairs experience a flattening during electronic excitation. More data about the change of geometry are given in the next section, where the forces acting on each atom after electronic excitation of the complex ion are calculated.

V. Excited-State Geometry

To analyze the question as to why the transition $^1B_g \leftarrow {}^1A_g$ exhibits one main progression in the measured absorption spectra, we have calculated the distorting forces acting on each of the atoms of the complex (especially of the skeleton $Co(CN)_2(N_2C_3)_2$ that results from the excitation of an electron from a t_2 into an e orbital. This will permit us to obtain a reasonable picture of the ^1B_g excited-state distortion relative to that of the ground state ^1A_g. The forces exerted in the electronic excited state ^1B_g with respect to the ^1A_g ground state are given by[9]

$$F_A = -\left\langle {}^1B_g \left| \frac{\partial H}{\partial \mathbf{R}_A} \right| {}^1B_g \right\rangle + \left\langle {}^1A_g \left| \frac{\partial H}{\partial \mathbf{R}_A} \right| {}^1A_g \right\rangle \qquad (3)$$

where $\mathbf{R}_A = (x_A, y_A, z_A)$ is the vector of three cartesian displacements of atom A taken in directions of the x, y, and z octahedral axes. The calculation has been carried out by means of the semiempirical molecular orbital (exteded Hückel) method, using SCF basis sets built up from STO. In particular, the 4s SCF function was expanded in four s-STO, the 4p functions into three p-STO, and the 3d functions consisted of two d-STO. Exponents and coefficients of the four s-STO, exponents of the two innermost p-STO, and exponents and coefficients of the two d-STO were chosen to minimize the energy E_{Av} of the configuration $3d^74s^2$; outermost p exponents and 4p-SCF coefficients were determined by optimizing the energy of the configuration $3d^74s4p$. The coefficients and exponents for the C and N SCF orbitals were determined by optimizing E_{Av} of the s^2p^2 and sp^3 configurations, respectively. The diagonal Hamiltonian matrix elements appropriate to the basis function at Co, H_{ii}, have been calculated according the method of Basch et al.[10a] and for the remaining

(7) Kanamori, K.; Ichinose, H.; Kawai, K. *Bull. Chem. Soc. Jpn.* **1982**, *55*, 1315. Here, the IR (solid) and Raman (aqueous solution) spectra of *trans*-$[Co(CN)_2(tn)_2]Cl\cdot H_2O$ between 400 and 550 cm^{-1} were reported. The IR spectrum in this paper coincides with that of the trihydrate in the present study, although detailed conditions of recrystallization of the compound were not given.

(8) Matsumoto, K.; Ooi, S.; Kuroya, H. *Bull. Chem. Soc. Jpn.* **1971**, *43*, 1903.

(9) Hurley, A. C. *Proc. R. Soc. London, A* **1954**, *170* (No. 226), 179.

(10) (a) Basch, H.; Viste, A.; Gray, H. B. *Theor. Chim. Acta* **1965**, *3*, 458. (b) Anno, T. *Theor. Chim. Acta* **1970**, *18*, 223.

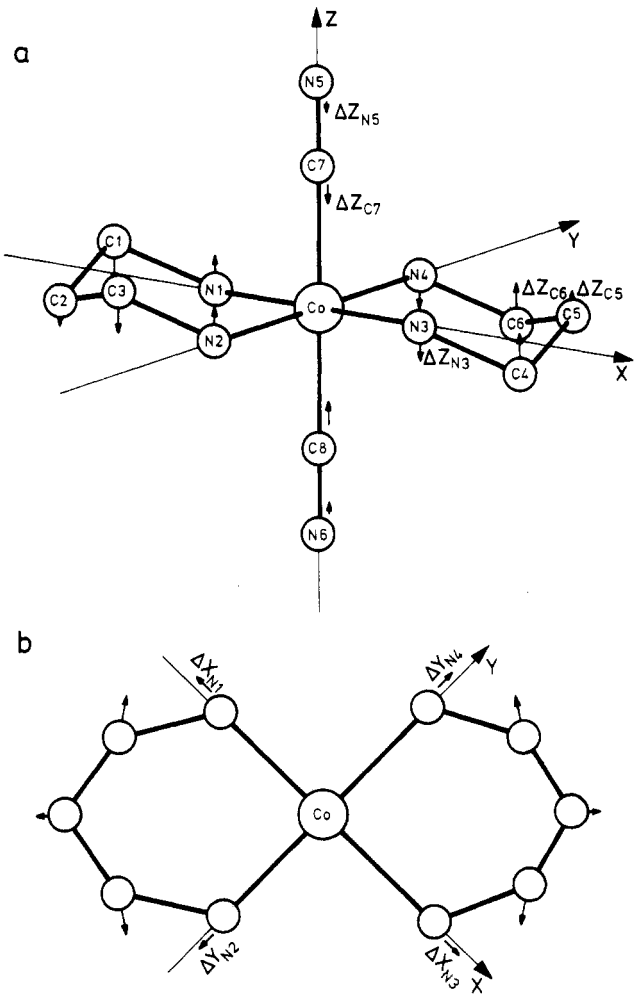

Figure 7. Distortion of the skeleton $Co(CN)_2(N_2C_3)_2$ in the excited ^1B_g state of the trihydrate crystal summarized in Table V: (a) along the z axis; (b) in the xy plane.

elements according to Anno,[10b] whereas the off-diagonal matrix elements H_{ij} were obtained from the Wolfsberg–Helmhotz formula with $K = 1.75$. One- and two-center intergrals that appear in the calculation of the forces were evaluated exactly by formulas given by Döring,[11] whereas three-center integrals were calculated in the point-charge approximation.[11] The Cartesian components of F_A for the transition $^1B_g \leftarrow {}^1A_g$ are listed in Table V. The forces acting on the corresponding atoms that are equivalent with respect to symmetry of the complex (C_{2h}) are the same but have to be taken with opposite signs. These forces give a ^1B_g state distortion (relative to the ground ^1A_g state) which is spectroscopically manifested in the occurrence of one main progression in the ν_δ' normal mode, for which $\Delta Q_\delta \neq 0$. At that distorted geometry ΔQ_δ, the force is balanced by the harmonic restoring force $k_\delta \Delta Q_\delta$,[12] $k_\delta \Delta Q_\delta + \sum_A F_A = 0$, where k_δ is the force constant associated with the δ mode. Here the summation is taken over all atoms of the skeleton $Co(CN)_2(N_2C_3)_2$. Although we do not know all distortions ΔQ_μ along other normal coordinates Q_μ, it is clear that $|\Delta Q_\mu| \ll |\Delta Q_\delta|$, which is the requirement for these modes to be negligible as distorting modes. If this does not hold, the restoring force $k_\mu \Delta Q_\mu$ must be added to the restoring force $k_\delta \Delta Q_\delta$ to balance the whole distorting force $\sum_A F_A$. Using the value of $k_\delta = 1.27$ mdyn/Å determined by the normal-coordinate analysis in the previous section, we obtain reasonable estimates of the magnitude and direction of the excited-state distortion in this mode. This is summarized in Table V in terms of the displacements Δx_A, Δy_A, and Δz_A of atoms A in the directions of the octahedral (molecular) axes x, y, and z (taken relative to the ground-state equilibrium geometry) and shown in Figure 7. In Figure 7 we see an elongation of the Co–N bonds (i.e., the signs of Δx_N and Δy_N being positive) and a shortening of the CoC bonds in the octahedral skeleton CoC_2N_4, associated with a slight N–C bond shortening and a C–C bond lengthening in the propanediamine ligands. At the same time the distance between the Co ion and the central C atom in the ring is nearly unaltered. Simultaneously with the tn ring moving out along the $x + y$ molecular axes, the N atoms and the C atoms in the chelate rings are shifted in the direction of the molecular z axis in an opposite phase, causing a flattening of the chelate ring chairs as discussed in the previous section.

The cyanide ligands move in, leading to a significant shortening of ≈0.1 Å of the metal–ligand Co—C≡N bond length in the excited state ^1B_g (relative to the ground state ^1A_g). This is much larger than that obtained from the spectral analysis (see below) and reported by Wilson and Solomon for the octahedral complex $Co(NH_3)_6^{3-}$ in $[Co(NH_3)_6](ClO_4)_2Cl{\cdot}KCl$, which upon excitation in the $^1T_{1g}$ state exhibits a D_{4h} equatorially expanded geometry.[13] On the basis of a spectral analysis of the transition $^1T_{1g} \leftarrow {}^1A_{1g}$, they have obtained an estimate for the change in axial Co–N bond length of ≈0.02 Å. Therefore, the surprisingly large shift of the cyanide ligands obtained by calculations must be treated with caution. Possibly this discrepancy arises from the fact that, according to eq 3, the force calculations comprise all totally symmetric modes, including the δ(tn cycle) mode, whereas the restoring force was taken solely along the δ mode. This may lead to errors in the magnitude of the distortion in some parts of the molecular skeleton, e.g. A, where the force F_A is balanced by several restoring forces. When a further restoring force $k_\mu \Delta Q_\mu$ is added to the restoring force $k_\delta \Delta Q_\delta$, where Q_μ has large contributions of CoC and C≡N stretching coordinates, the distoring force F_A acting on the cyanide ligands can be balanced by a shorter stretch Co—C≡N. Such modes were found by calculation to have ground-state frequencies of 406 cm^{-1} (experimentally determined as 412 cm^{-1}; see Table III) and 2122 cm^{-1}. They have such small displacements that their progressions are too short to cause any significant effect on the main ν_δ progression. Qualitatively, the distortions are similar for the low-symmetry complex in the monohydrate crystal, although the atomic displacements are not presented here.

Using for comparison the experimentally determined value ΔQ_δ = 0.32 Å and reexpressing the internal coordinates in terms of normal coordinates by means of the **L** matrix, one finds the relative change in the bond length Co–N and the axial shift of the N atoms to be $\Delta x_{N3} = \Delta y_{N4} = 0.061$ Å and $\Delta z_{N3} = \Delta z_{N4} = -0.06$ Å, respectively. The latter are deduced from the change of the bending coordinate δ(C7CoN3(4)) involved in the ν_δ mode. (This agrees fairly well with $\Delta x_{N3} = \Delta y_{N4} = -\Delta z_{N3} = -\Delta z_{N4} = -0.071$ Å of Table V.) Simultaneously with an elongation of the Co–N bonds, the C–N bond in the chelate ring will be shortened by ≈0.02 Å (~0.1 Å by calculation), whereas the C–C bond remains practically unchanged (lengthened by calculations). Furthermore, the cyanide ligands shift toward the central ion, leading to a contraction of ≈0.03 Å. At the same time the C≡N bond length remains practically unchanged. This shows that while there is tolerable agreement with calculated bond lengthening, the significant difference occurs mainly in the contraction along the vertical axis and in the C–C bond length change in the chelate rings. To correct for these errors we have to reestimate the restoring (rather than the distorting) forces in these parts of the molecular skeleton to obtain our relative atomic displacements. Finally, we should say that calculations cannot provide data with an accuracy achieved by the best experiment, so that one should look to calculations primarily to provide information on those parts of the molecular skeleton that are not easily probed by experiment.

VI. Summary

In conclusion, we would like to point out that the main features of the structure in the region of the lowest spin-allowed transition in *trans*-$[Co(CN)_2(tn)_2]^+$ are understood. The electronic ab-

(11) Döring, U. Ph.D. Thesis, University of Bochum, 1978.
(12) Wilson, R. B.; Solomon, E. I. *Inorg. Chem.* **1978**, *17*, 1729.
(13) Wilson, R. B.; Solomon, E. I. *J. Am. Chem. Soc.* **1980**, *102*, 4085.

sorption spectra show one main progression in a ν_δ' normal mode, which means that the only strong force exerted in the excited-state conformations ^1B_g (trihydrate) and ^1A (monohydrate) is along the Q_δ coordinate. This results in a motion outward of the propanediamine ligands along the $x + y$ molecular axes, which is realistic since the lowest energy transition involves promotion to an antibonding $d_{x^2-y^2}$ orbital, which has four lobes pointing along the x and y molecular axes containing the N atoms. Therefore, the force (eq 3) will have an appreciable amplitude along such normal coordinates Q, for which the gradient $\partial H/\partial Q = \partial V/\partial Q$ of the dynamic ligand field exhibits the same directional property. This condition is best fulfilled by the ν_δ mode, because of the sizable contribution of Co–N bond stretching coefficients to this mode.

Apart from the Q_δ mode, there are further normal modes of vibrations that involve comparable amounts of Co–N bond stretching and that therefore might have the same significance as Q_δ. However, in comparison with the latter, these normal modes involve larger contributions of Co–C, C–N and C–C stretching coordinates and therefore exhibit greater force constants. These greater force constants lead to greater resistance to distortion, and hence the corresponding displacements become small and are not measurable. This means that even if those modes are mixed with the ν_δ mode, resulting in rotation of their normal coordinates in the excited state relative to the normal modes in the ground state (i.e., the Dushinsky effect[5,14]), they contribute only negligibly to the absorption band.

Acknowledgment. We are indebted to Dr. F. Mark for providing the extended Hückel program. H.K. wishes to thank Professor O. E. Polansky for continuing support of this work. We also thank Professor H.-H. Schmidtke of the University of Düsseldorf, where preliminary measurements of low-temperature absorption spectra of some crystals were done. This research was supported by the Scientific Research Fund of the Ministry of Education of Japan and by the Fonds der Chemischen Industrie Frankfurt (Main), Germany.

Supplementary Material Available: Listings of final atomic fractional coordinates, thermal parameters, and interatomic distances and angles (3 pages); a listing of observed and calculated structure factors (12 pages). Ordering information is given on any current masthead page.

(14) Dushinsky, F. *Acta Physicochim. URSS* **1937**, *7*, 51.

Contribution from the Ministero della Pubblica Istruzione of Italy, Dipartimento di Chimica, University of Modena, 41100 Modena, Italy, Istituto di Chimica Generale e Inorganica and Centro per la Strutturistica Diffrattometrica del CNR, University of Parma, 43100 Parma, Italy, and Istituto di Chimica Generale e Inorganica, University of Sassari, 07100 Sassari, Italy

Coordination Behavior of N-Protected Aspartic Acid in Binary and Ternary Copper(II) Complexes. Crystal and Molecular Structure of Bis(2,2′-bipyridine)bis(μ-*N*-(benzyloxycarbonyl)-L-aspartato-*O*,*O*′,*O*″)dicopper(II)–2.5-Water–0.5-Sodium Perchlorate

L. Antolini,[1a] L. P. Battaglia,[1b] A. Bonamartini Corradi,[1b] L. Menabue,[1a] G. Micera,*[1c] and M. Saladini[1a]

Received January 14, 1985

The complexes $[Cu(Z\text{-asp})(H_2O)]_n \cdot 0.25n NaClO_4$ (Z-asp = *N*-(benzyloxycarbonyl)-L-aspartato), $[Cu(Ac\text{-asp})(H_2O)]_n \cdot nH_2O$ (Ac-Asp = *N*-acetyl-L-aspartato), and $[Cu(Bz\text{-asp})(H_2O)]_n \cdot 1.5nH_2O$ (Bz-asp = *N*-benzoyl-L-aspartato) were synthesized and characterized by means of spectroscopic and magnetic measurements. The results substantiate dimeric structures of the copper(II) acetate monohydrate type without strong magnetic interactions between the Cu–Cu couples. Mixed complexes with 2,2′-bipyridine were also obtained and characterized. For one of them, $[Cu(Z\text{-asp})(bpy)]_2 \cdot 2.5H_2O \cdot 0.5NaClO_4$, the crystal structure was determined by X-ray diffraction. The compound crystallizes in the monoclinic space group $P2_1$ in a cell of dimensions a = 18.603 (2) Å, b = 12.943 (1) Å, c = 20.945 (2) Å, and β = 106.65 (1)°. The calculated density (1.479 g cm^{-3}) is consistent with four dimeric units in the unit cell. The structure was solved by Patterson and Fourier methods and refined by least-squares calculations to a conventional R factor of 0.078 for 7970 counter data. It consists of two crystallographically independent $Cu_2(Z\text{-asp})_2(bpy)_2$ molecules, one Na^+ interacting with carboxylate oxygens, a ClO_4^- anion weakly hydrogen bonded to a water molecule, and five lattice water molecules. The binuclear complex molecules result through bridge formation between two metal atoms by the α- and β-carboxylate groups of two aspartate ions. The four copper ions exhibit severely distorted, but similar, square-pyramidal coordination geometries. The aspartate ion, whose β-carboxylate group acts as an axial and equatorial bidentate ligand, shows an unusual metal binding mode, which may be attributed to the presence of Na^+. The crystal packing is determined by hydrogen-bonding interactions and by two different systems of combined ring stacking and hydrophobic interactions involving all the aromatic moieties of the complex molecules. Spectroscopic results suggest that the metal coordination geometry is the same in all the ternary complexes.

Introduction

Side-chain carboxylic groups of biomolecules are important sites for metal binding. However, their involvement in coordination depends on the nature of the other binding sites available for the metal. Particularly, potentially tridentate amino acids with a carboxylic group as the third donor site, such as aspartic and glutamic acids, exhibit only limited tendency to form tridentate chelates in aqueous solution and often coordinate essentially in the bis(glycinato)-like way.[2-5] A similar behavior was observed, in the solid state, with Cu(II) only for highly hydrated ternary complexes existing as isolated monomeric species. In anhydrous or low-hydrate complexes, polymeric chain structures are always present, where aspartate and glutamate ions, in an extended configuration, bridge two or three different copper(II) ions.[6]

(1) (a) University of Modena. (b) University of Parma. (c) University of Sassari.

(2) Nagypal, I.; Gergely, A.; Farkas, E. *J. Inorg. Nucl. Chem.* **1974**, *36*, 699.
(3) Harrison, M. R.; Rossotti, F. J. C. *J. Chem. Soc., Chem. Commun.* **1970**, 175.
(4) Brookes, G.; Pettit, L. D. *J. Chem. Soc., Dalton Trans.* **1977**, 1918.
(5) Claridge, R. F.; Kilpatrick, J. J.; Powell, H. K. J. *Aust. J. Chem.* **1980**, *33*, 2757.

0020-1669/86/1325-3301$01.50/0